

# KIC 11401845: An Eclipsing Binary with Multiperiodic Pulsations and Light Travel Time

Jae Woo Lee<sup>1,2</sup>, Kyeongsoo Hong<sup>1</sup>, Seung-Lee Kim<sup>1,2</sup>, and Jae-Rim Koo<sup>1</sup>

<sup>1</sup>*Korea Astronomy and Space Science Institute, Daejeon 34055, Korea*

<sup>2</sup>*Astronomy and Space Science Major, Korea University of Science and Technology, Daejeon 34113, Korea*

jwlee@kasi.re.kr, kshong@kasi.re.kr, slkim@kasi.re.kr, koojr@kasi.re.kr

## ABSTRACT

We report the *Kepler* photometry of KIC 11401845 displaying multiperiodic pulsations, superimposed on binary effects. Light-curve synthesis represents that the binary star is a short-period detached system with a very low mass ratio of  $q = 0.070$  and filling factors of  $F_1 = 45\%$  and  $F_2 = 99\%$ . Multiple frequency analyses were applied to the light residuals after subtracting the synthetic eclipsing curve from the observed data. We detected 23 frequencies with signal to noise amplitude ratios larger than 4.0, of which the orbital harmonics ( $f_4, f_6, f_9, f_{15}$ ) in the low frequency domain may originate from tidally excited modes. For the high frequencies of  $13.7\text{--}23.8\text{ day}^{-1}$ , the period ratios and pulsation constants are in the ranges of  $P_{\text{pul}}/P_{\text{orb}} = 0.020\text{--}0.034$  and  $Q = 0.018\text{--}0.031\text{ d}$ , respectively. These values and the position on the Hertzsprung-Russell diagram demonstrate that the primary component is a  $\delta$  Sct pulsating star. We examined the eclipse timing variation of KIC 11401845 from the pulsation-subtracted data and found a delay of  $56 \pm 17\text{ s}$  in the arrival times of the secondary eclipses relative to the primary eclipses. A possible explanation of the time shift may be some combination of a light-travel-time delay of about  $34\text{ s}$  and a very small eccentricity of  $e \cos \omega < 0.0002$ . This result represents the first measurement of the Rømer delay in non-compact binaries.

*Subject headings:* binaries: eclipsing — stars: fundamental parameters — stars: individual (KIC 11401845) — stars: oscillations (including pulsations)

## 1. INTRODUCTION

The *Kepler* satellite provides the highly precise and nearly-continuous photometric data for  $\sim 200,000$  objects that has helped to revolutionize the study of stars themselves, as well as extrasolar planets (Borucki et al. 2010; Koch et al. 2010). There are 2878 eclipsing and ellipsoidal binaries in the *Kepler* main field of view (Kirk et al. 2016), corresponding to about 1.3% of all observed targets.

Eclipsing binaries (EBs) serve as critical tools that provide an accurate and direct determination of fundamental stellar parameters such as the mass and radius for each component. These data allow us to test stellar evolution models and to determine distances of binary systems (Torres et al. 2010). Furthermore, it is possible to measure precisely mid-eclipse times from binary light curves. The timing measurements are used to investigate a variety of physical phenomena causing the orbital period changes of EBs (Hilditch 2001; Kreiner et al. 2001). Such examples are mass transfer, angular momentum loss, apsidal motion in an elliptical orbit, third-body effect, and magnetic activity cycle.

EBs with pulsating components are very promising objects for the study of stellar structure and evolution, because binarity provides useful information about the components and asteroseismology assists in probing the interiors of stars. Most of them have been found to be  $\delta$  Sct-type pulsators of classical semi-detached Algols (Mkrtychian et al. 2004; Liakos & Niarchos 2016b). The  $\delta$  Sct stars are dwarfs and subgiants with spectral types A and F located in the lower portion of the Cepheid instability strip. They pulsate in low-order pressure ( $p$ ) modes with typical periods of 0.02–0.25 days and amplitudes of less than 0.1 mag (Breger 2000; Rodríguez & Breger 2001). The pulsations are driven by the  $\kappa$  mechanism mostly due to partial ionization of He II. The  $\delta$  Sct variables in binaries have pulsation features similar to single  $\delta$  Sct stars, but their pulsations can be affected by mass transfer between both components and gravitation forces from companions. Recently, Liakos & Niarchos (2015, 2016a) showed that there is a threshold in the orbital period of  $\sim 13$  days below which the pulsations are influenced by the binarity. In eccentric-orbit binaries, some pulsations can be excited by tidal interaction. The signature of the tidally excited modes is the frequencies at multiples of the orbital frequency (Welsh et al. 2011; Hambleton et al. 2013).

This paper is the fifth contribution in a series of detailed studies for pulsating stars in the *Kepler* EBs (Lee et al. 2014, 2016a,b; Lee 2016). We present that KIC 11401845 (R.A.<sub>2000</sub> = 19<sup>h</sup>25<sup>m</sup>11<sup>s</sup>.275; decl.<sub>2000</sub> = +49°14′40″.09;  $K_p$  = +14.355;  $g$  = +14.443;  $g - r$  = +0.118) is a detached EB exhibiting multiperiodic pulsations and light-travel-time (LTT) delay. The system was announced to be an EB pulsating at frequencies of 13–25 d<sup>-1</sup> by Gaulme & Guzik (2014).

## 2. KEPLER PHOTOMETRY AND LIGHT-CURVE SYNTHESIS

The *Kepler* data of KIC 11401845 were obtained in a long cadence mode of 29.42 minutes during Quarters 10 and 12. We used the SAP (Simple Aperture Photometry) time-series data in Data Release 25 retrieved from the *Kepler* Data Archive<sup>1</sup>. The raw data were detrended by using second-order polynomials that were separately applied to each quarter. As eclipses influence the detrending process, we fitted the polynomial to only the outside-eclipse part of the light curve (e.g., Hambleton et al. 2013). The flux measurements were converted to a magnitude scale by requiring

---

<sup>1</sup><http://archive.stsci.edu/kepler/>

a *Kepler* magnitude of +14.355 at maximum light. The detrended *Kepler* data are displayed in Figure 1. The shape of the light curve indicates a significant temperature difference between the binary components and an ellipsoidal variation due to tidal distortions.

To derive the binary parameters of this system, all *Kepler* data were analyzed using the Wilson-Devinney binary program (Wilson & Devinney 1971, van Hamme & Wilson 2007; hereafter W-D). This synthesis was performed in a way similar to that for the pulsating EBs V404 Lyr (Lee et al. 2014) and KIC 6220497 (Lee et al. 2016a). The effective temperature of the hotter and more massive star was set to be 7590 K from the *Kepler* Input Catalogue (KIC; Kepler Mission Team 2009). The logarithmic bolometric ( $X_{1,2}$ ) and monochromatic ( $x_{1,2}$ ) limb-darkening coefficients were interpolated from the values of van Hamme (1993). In Table 1, the parentheses signify the adjusted parameters. In this article, the subscripts 1 and 2 refer to the primary and secondary components being eclipsed at orbital phases 0.0 (Min I) and 0.5 (Min II), respectively.

There has been neither a light-curve solution nor spectroscopic mass ratio ( $q$ ) for KIC 11401845 so far. Thus, we conducted a photometric  $q$ -search procedure that calculates a series of models with varying  $q$  from 0 to 1. For each assumed mass ratio, the W-D code was applied for various modes but converged satisfactorily only when detached mode 2 were used. The weighted sum of the squared residuals,  $\sum W(O - C)^2$ , reached a minimum around  $q = 0.07$ , which was adopted as the initial value and thereafter adjusted to derive the photometric solutions. The result is given as Model 1 in the second and third columns of Table 1. The synthetic light curve appears as the blue solid curve in Figure 1, and the corresponding light residuals are plotted as the gray ‘x’ symbols in the figure. In all the procedures, we considered an orbital eccentricity ( $e$ ) and a third light ( $l_3$ ) as additional free parameters. Both searches led to values for the two parameters which were zero within their errors, which implies that KIC 11401845 has negligible eccentricity. We obtained the errors for the adjustable parameters by splitting the *Kepler* data into 79 segments at intervals of an orbital period and analyzing them separately (Koo et al. 2014). In Table 1, the error of each parameter is its standard deviation computed from this process.

Absolute parameters for KIC 11401845 can be computed from our light-curve solutions in Table 1 and from the correlations between spectral type (temperature) and stellar mass. The surface temperature ( $T_1 = 7590$  K) of the primary star corresponds to a normal dwarf one with a spectral type of  $\sim$ A8V. Assuming that each component has a temperature error of 200 K, the primary’s mass was estimated to be  $M_1 = 1.70 \pm 0.08 M_\odot$  from Harmanec’s (1988) empirical relation. We calculated the absolute dimensions for each component given in the last part of Table 1. Here, the luminosity ( $L$ ) and bolometric magnitudes ( $M_{\text{bol}}$ ) were derived by using  $T_{\text{eff}\odot} = 5780$  K and  $M_{\text{bol}\odot} = +4.73$ . The bolometric corrections (BCs) were obtained from the expression between  $\log T_{\text{eff}}$  and BC given by Torres (2010).

Considering the temperature error of the primary star, we carried out the light-curve synthesis for 7390 K and 7790 K. The binary parameters from the two limits are in satisfactory agreement with those from  $T_1 = 7590$  K, except for the secondary’s temperature ( $T_2$ ). In the three models, the

temperature ratios ( $T_2/T_1$ ) of both components are consistent with each other within their errors. We can see that the adopted  $T_1$  does not affect the results presented in this paper.

### 3. LIGHT RESIDUALS AND PULSATONAL CHARACTERISTICS

From the temperature ( $T_1$ ) and surface gravity ( $\log g_1$ ) given in Table 1, the primary star of KIC 11401845 resides within the  $\delta$  Sct instability strip and, hence, it would be a candidate for  $\delta$  Sct pulsations. For more reliable frequency analysis, we followed the procedure described by Lee (2016). First, we divided the observed *Kepler* data of KIC 11401845 into 79 subsets as before and modeled each light curve with the W-D code by adjusting only the ephemeris epoch ( $T_0$ ) in Model 1 of Table 1. Second, the corresponding residuals from the whole datasets were applied to multiple frequency analyses in the range from 0 to the Nyquist limit of  $f_{Ny} = 24.4 \text{ day}^{-1}$  using the PERIOD04 program (Lenz & Breger 2005). Because the binary components block each other’s lights during eclipses, we used only the outside-eclipse residuals (orbital phases 0.07–0.43 and 0.57–0.93). According to the successive prewhitening procedures, we detected the frequencies with signal to noise amplitude (S/N) ratios larger than 4.0 (Breger et al. 1993). Third, we solved the pulsation-subtracted data after removing the pulsations from the observed data. As a result, new binary parameters were obtained, and they were used to reanalyze the 79 light curves in the first stage.

This process was repeated three times until the detected frequencies were unchanged. Final binary parameters are given as Model 2 in the fourth and fifth columns of Table 1, and the pulsation-subtracted data and model light curve are plotted in Figure 2. We can see that the physical parameters for Model 2 are consistent with those for Model 1. Figure 3 shows the light residuals after removal of the binary effects from the observed *Kepler* data. We detected a total of 23 frequencies larger than the empirical threshold of  $S/N = 4.0$ . The amplitude spectra before and after prewhitening the first 10 frequencies and then all 23 frequencies are shown in the first to third panels of Figure 4, respectively. The detailed result from the frequency analysis is listed in Table 2, where the frequencies are given in order of detection and the noises are calculated in the range of 5  $\text{day}^{-1}$  around each frequency. The uncertainties in the table were obtained according to Kallinger et al. (2008). The synthetic curve computed from the 23-frequency fit is displayed in the lower panel of Figure 3.

As listed in Table 2, four in the low-frequency region ( $0.4\text{--}3.8 \text{ day}^{-1}$ ) and 19 in the high-frequency region ( $13.7\text{--}23.8 \text{ day}^{-1}$ ) were derived from the multiple frequency analyses of the outside-eclipse light residuals. Within the frequency resolution of  $0.00545 \text{ day}^{-1}$  (Loumos & Deeming 1978), we searched the frequencies for possible harmonic and combination terms. The result is given in the last column of Table 2. We think that the  $f_{11}$  to  $f_{23}$  frequencies mainly arise from combination frequencies, some of which can be caused by imperfect removal of the binary effects in the observed data. On the other hand, the high-frequency signals close to the Nyquist limit can be reflections of real frequencies ( $2f_{Ny} - f_i$ ) higher than  $f_{Ny}$  (Murphy et al. 2013; Lee et al. 2016b). High-cadence photometry is needed to separate the Nyquist aliases from the detected frequencies

of KIC 11401845.

#### 4. ECLIPSE TIMING VARIATION AND ITS IMPLICATION

For an orbital period study of KIC 11401845, we determined 150 minimum times and their uncertainties from the observations with the method of Kwee & van Woerden (1956). These minima are listed in columns (1)–(5) of Table 3, where we present the cycle numbers and  $O-C_1$  residuals calculated with the light elements ( $T_0$  and  $P$ ) for Model 2 in Table 1. The resultant eclipse timing diagram is displayed at the top panel of Figure 5. As shown in the figure, the timing residuals from the primary (filled circle) and secondary (open circle) eclipses do not agree with each other, which could be caused by the light variations due to the multiperiodic pulsations of the primary star. Thus, we recalculated the minimum times from the eclipse light curve after subtracting the 23 frequencies detected in Section 3 from the observed *Kepler* data. The results are given in columns (6)–(8) of Table 3 and are illustrated in the middle panel of Figure 5.

As displayed in Figure 5, the large discrepancy between Min I and Min II is shown more clearly in the pulsation-subtracted data. This discrepancy can result from the time difference between the primary and secondary eclipses due to LTT in a binary with unequal masses (Barlow et al. 2012; Parsons et al. 2014). The Rømer delay is given by Kaplan (2010), as follows:

$$\Delta t_{\text{LTT}} = \frac{PK_2}{\pi c}(1 - q), \quad (1)$$

where  $P$  is the orbital period,  $K_2$  is the radial velocity (RV) semi-amplitude of the secondary star, and  $c$  is the speed of light. From the Model 2 parameters in Table 1, we derived the velocities ( $K_1 = 13 \text{ km s}^{-1}$  and  $K_2 = 187 \text{ km s}^{-1}$ ) of the binary components (Hilditch 2001). The time delay of  $\Delta t_{\text{LTT}} = 34 \pm 1 \text{ s}$  was obtained by applying the values of  $K_2$ ,  $P$ , and  $q$  to equation (1).

In order to examine this possibility, we computed the secondary eclipses related to one half period after the primary eclipses in the pulsation-subtracted data and then plotted the difference ( $\Delta t_{\text{SE}}$ ) between the measured and computed secondary times in the bottom panel of Figure 5. As shown in the figure, the mean value is offset from zero and gives a time delay of  $\Delta t_{\text{SE}} = 56 \pm 17 \text{ s}$  in the secondary eclipse. This value is calculated to be  $\Delta t_{\text{SE}} = 37 \pm 27 \text{ s}$  in the observed *Kepler* data including pulsations. Within their errors, the time delays of  $\Delta t_{\text{SE}}$  are in satisfactory accord with the predicted delay of  $\Delta t_{\text{LTT}}$ . On the other hand, if KIC 11401845 is in an eccentric orbit,  $\Delta t_{\text{SE}}$  might be affected by the time shift of  $\Delta t_e$  in the secondary eclipse due to a non-zero eccentricity:

$$\Delta t_e \simeq \frac{2Pe}{\pi} \cos \omega, \quad (2)$$

$$\Delta t_{\text{SE}} \simeq \Delta t_e + \Delta t_{\text{LTT}}, \quad (3)$$

where  $e$  and  $\omega$  are the eccentricity and the argument of periastron, respectively. Using the equations (2) and (3),  $e \cos \omega \simeq 0.00003$  for the observed data and  $e \cos \omega \simeq 0.00019$  for the pulsation-subtracted data.

## 5. DISCUSSION AND CONCLUSIONS

We have studied the physical properties of KIC 11401845, based on the *Kepler* data made during Quarters 10 and 12. The light curve of this system displays multiperiodic pulsations, superimposed on binary effects. To examine whether the binary parameters are affected by the pulsations, we analyzed individually the observed and pulsation-subtracted *Kepler* data with the W-D code. As listed in Table 1, the photometric solutions for the two datasets are in good agreement with each other, which means that the pulsations cause little impact on the light-curve parameters. Our light-curve synthesis shows that KIC 11401845 is a short-period detached EB with a very small mass ratio of about 0.07. The primary and secondary components fill  $F_1 = 45\%$  and  $F_2 = 99\%$  of their limiting lobe, respectively, where the filling factor  $F_{1,2} = \Omega_{\text{in}}/\Omega_{1,2}$ . With its small  $q$  and short  $P$ , our program target closely resembles the two *Kepler* pulsating EBs KIC 10661783 (Lehmann et al. 2013) and KIC 8262223 (Guo et al. 2016), which are detached binaries with characteristics of the R CMa-type stars (Budding & Butland 2011; Lee et al. 2016b) among Algols. A comparison of the KIC 11401845 parameters with the mass-radius, mass-luminosity, and Hertzsprung-Russell (HR) diagrams (Ibanoglu et al. 2006) shows that the primary component resides within the main-sequence band. On the contrary, the low mass secondary is highly evolved and its radius and luminosity are remarkably oversized and overluminous compared to main-sequence stars of the same mass. These suggest that the initial more massive star becomes the present secondary by losing most of its own mass via mass transfer to the companion (present primary) and stellar wind (Hong et al. 2015; Guo et al. 2016).

In order to detect the pulsation frequencies of KIC 11401845, multiple frequency analyses were applied to the out-of-eclipse residuals after removing the binarity effects from the observed *Kepler* data. We found 23 frequencies with S/N ratios larger than 4.0 in two regions: 0.4–3.8 day<sup>-1</sup> and 13.7–23.8 day<sup>-1</sup>. Among these, four ( $f_4, f_6, f_9, f_{15}$ ) in the low frequency region are frequencies at exact multiples of the orbital frequency,  $f_{\text{orb}} = 0.46267$  day<sup>-1</sup>. The orbital harmonics can be attributed to tidally excited modes, which occur when the orbital frequency is close to a stellar eigenfrequency in a binary star (Welsh et al. 2011; Hambleton et al. 2013). On the contrary, the other frequencies are strongly reminiscent of the  $p$ -mode pulsations known in EBs (e.g., Southworth et al. 2011; Lee et al. 2016b). The ratios of the pulsational to orbital periods in the high-frequency region were calculated to be  $P_{\text{pul}}/P_{\text{orb}} = 0.020\text{--}0.034$ , which is within the upper limit of 0.09 for  $\delta$  Sct stars in binaries (Zhang et al. 2013). We calculated the pulsation constants by applying the Model 2 parameters in Table 1 to the equation of  $\log Q_i = -\log f_i + 0.5 \log g + 0.1 M_{\text{bol}} + \log T_{\text{eff}} - 6.456$  (Petersen & Jørgensen 1972). The result is listed in the sixth column of Table 2. The  $Q$  values of 0.018–0.031 d correspond to  $p$  modes of  $\delta$  Sct type. The period ratios, the pulsation constants, and the position on the HR diagram reveal that the primary component is a  $\delta$  Sct variable. The  $\delta$  Sct pulsations of KIC 11401845 match well the correlations between the pulsation periods and other parameters (binary periods, surface gravities of pulsators, and gravitational forces from companions) updated by Liakos & Niarchos (2016b).

We measured the minimum epochs of the primary and secondary eclipses from the observed

and pulsation-subtracted data. Inspecting them in detail, we found delays of about 37 s and 56 s in the arrival times of the secondary eclipses relative to the primary eclipses in the same order. The values are consistent with the expected time delay of  $\Delta t_{\text{LTT}} = 34$  s across the binary orbit. This indicates that the LTT delay is the main cause of the time discrepancy between both eclipses, which is the first detection of this effect in EBs consisting of non-compact components. One might imagine that the time delay of the secondary eclipse could be apportioned between the LTT delay and a non-zero eccentricity. The result presented in this paper limits the eccentricity of KIC 11401845 to  $e < 0.0002$ . When the high-resolution spectra are made, they will help to determine the RV semi-amplitudes ( $K_{1,2}$ ) and mass ratio ( $q$ ) of the binary star and hence to derive its small eccentricity ( $e$ ). Because the system is a faint pulsating EB with a short orbital period, 8–10 m class telescopes are required to measure its accurate double-lined RVs.

This paper includes data collected by the *Kepler* mission. *Kepler* was selected as the 10th mission of the Discovery Program. Funding for the *Kepler* mission is provided by the NASA Science Mission directorate. We have used the Simbad database maintained at CDS, Strasbourg, France. This work was supported by the KASI grant 2016-1-832-01. Work by K. Hong was supported by Basic Science Research Program through the National Research Foundation of Korea (NRF) funded by the Ministry of Education (grant number: NRF-2016R1A6A3A01007139).

## REFERENCES

- Barlow, B. N., Wade, R. A., & Liss, S. E. 2012, *ApJ*, 753, 101
- Breger, M. 2000, in *ASP Conf. Ser.* 210, *Delta Scuti and Related Stars*, ed. M. Breger, & M. H. Montgomery (San Francisco: ASP), 3
- Breger, M., Stich, J., Garrido, R., et al. 1993, *A&A*, 271, 482
- Borucki, W. J., Koch, D., Basri, G., et al. 2010, *Science*, 327, 977
- Budding, E., & Butland, R. 2011, *MNRAS*, 418, 1764
- Gaulme, P., & Guzik, J. A. 2014, in *Proc. IAU Symp.* 301, *Precision Asteroseismology*, ed. J. A. Guzik, W. Chaplin, G. Handler, & A. Pigulski (Cambridge: Cambridge Univ. Press), 413
- Guo, Z., Gies, D. R., Matson, R. A., Garcia Hernandez, A., Han, Z., & Chen, X. 2016, *ApJ*, submitted (eprint arXiv:1610.00350)
- Hambleton, K. M., Kurtz, D. W., Prša, A., et al. 2013, *MNRAS*, 434, 925
- Harmanec, P. 1988, *Bull. Astron. Inst. Czechoslovakia*, 39, 329
- Hilditch, R. W. 2001, *An Introduction to Close Binary Stars* (Cambridge: Cambridge Univ. Press)
- Hong, K., Lee, J. W., Kim, S.-L., et al. 2015, *AJ*, 150, 131
- İbanoğlu, C., Soyduğan, F., Soyduğan, E., & Dervişoğlu, A. 2006, *MNRAS*, 373, 435
- Kallinger, T., Reegen, P., & Weiss, W. W. 2008, *A&A*, 481, 571
- Kaplan, D. L. 2010, *ApJ*, 717, L108
- Kepler Mission Team 2009, *VizieR Online Data Catalog*, 5133, 0
- Kirk, B., Conroy, K., Prša, A., et al. 2016, *AJ*, 151, 68
- Koch, D. G., Borucki, W. J., Basri, G., et al. 2010, *ApJ*, 713, L79
- Koo, J.-R., Lee, J. W., Lee, B.-C., et al. 2014, *AJ*, 147, 104
- Kreiner, J. M., Kim, C.-H., & Nha, I.-S. 2001, *An Atlas of O–C Diagrams of Eclipsing Binary Stars* (Krakow: Wydawn. Nauk. Akad. Pedagogicznej)
- Kwee, K. K., & van Woerden, H. 1956, *Bull. Astron. Inst. Netherlands*, 12, 327
- Lee, J. W. 2016, *ApJ*, in press (eprint arXiv:1609.06387)
- Lee, J. W., Hong, K., Kim, S.-L., & Koo, J.-R. 2016a, *MNRAS*, 460, 4220



- Lee, J. W., Kim, S.-L., Hong, K., Koo, J.-R., Lee, C.-U., & Youn, J.-H. 2016b, *AJ*, 151, 25
- Lee, J. W., Kim, S.-L., Hong, K., Lee, C.-U., & Koo, J.-R. 2014, *AJ*, 148, 37
- Lehmann, H., Southworth, J., Tkachenko, A., & Pavlovski, K. 2013, *A&A*, 557, A79
- Lenz, P., & Breger, M. 2005, *Comm. Asteroseismology*, 146, 53
- Liakos, A., & Niarchos, P. 2015, in *ASP Conf. Ser.* 496, ed. S. M. Rucinski, G. Torres, & M. Zejda (San Francisco: ASP), 195
- Liakos, A., & Niarchos, P. 2016a, preprint (eprint arXiv:1606.08638)
- Liakos, A., & Niarchos, P. 2016b, *MNRAS*, in press (eprint arXiv:1611.00200)
- Loumos, G. L., & Deeming, T. J. 1978, *Ap&SS*, 56, 285
- Mkrtichian, D. E., Kusakin, A. V., Rodriguez, E., et al. 2004, *A&A*, 419, 1015
- Murphy, S. J., Shibahashi, H., & Kurtz, D. W., 2013, *MNRAS*, 430, 2986
- Parsons, S. G., Marsh, T. R., Bours, M. C. P., et al. 2014, *MNRAS*, 438, L91
- Petersen, J. O., & Jørgensen, H. E. 1972, *A&A*, 17, 367
- Rodríguez, E., & Breger, M. 2001, *A&A*, 366, 178
- Southworth, J., Zima, W., Aerts, C., et al. 2011, *MNRAS*, 414, 2413
- Torres, G. 2010, *AJ*, 140, 1158
- Torres, G., Andersen, J., & Giménez, A. 2010, *A&AR*, 18, 67
- Van Hamme, W. 1993, *AJ*, 106, 209
- Van Hamme, W., & Wilson, R. E. 2007, *ApJ*, 661, 1129
- Welsh, W. F., Orosz, J. A., Aerts, C., et al. 2011, *ApJS*, 197, 4
- Wilson, R. E., & Devinney, E. J. 1971, *ApJ*, 166, 605
- Zhang, X. B., Luo, C. Q., & Fu, J. N. 2013, *ApJ*, 777, 77

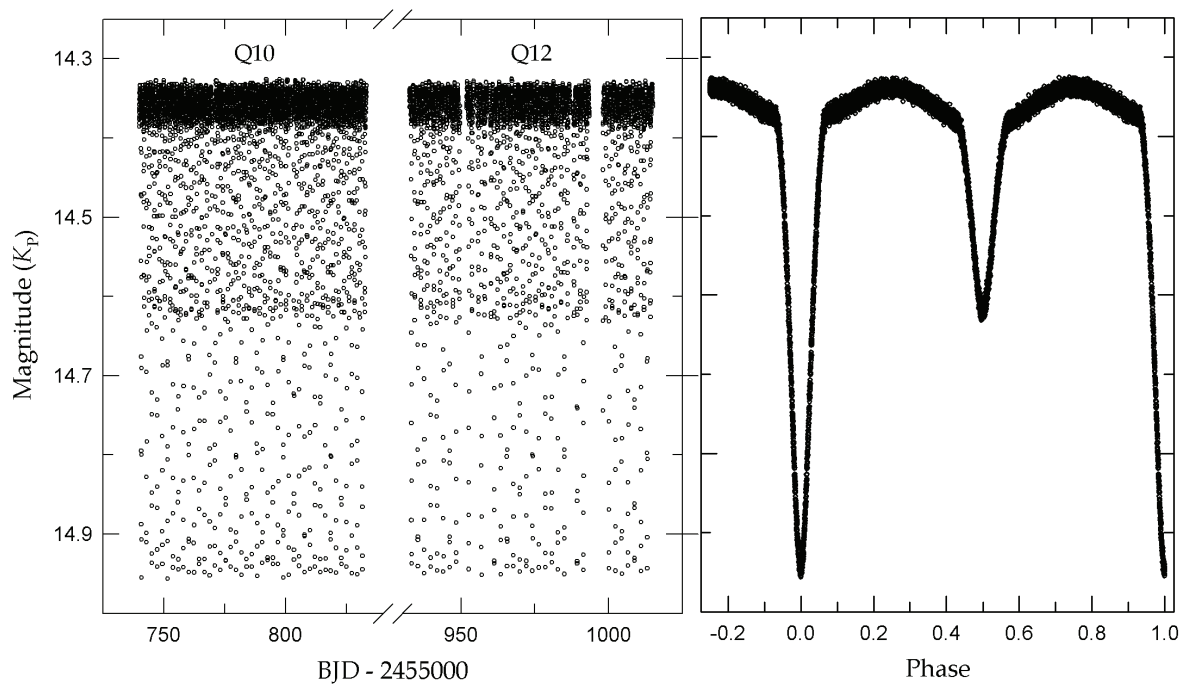


Fig. 1.— Detrended *Kepler* data of KIC 11401845 distributed in BJD (left panel) and orbital phase (right panel).

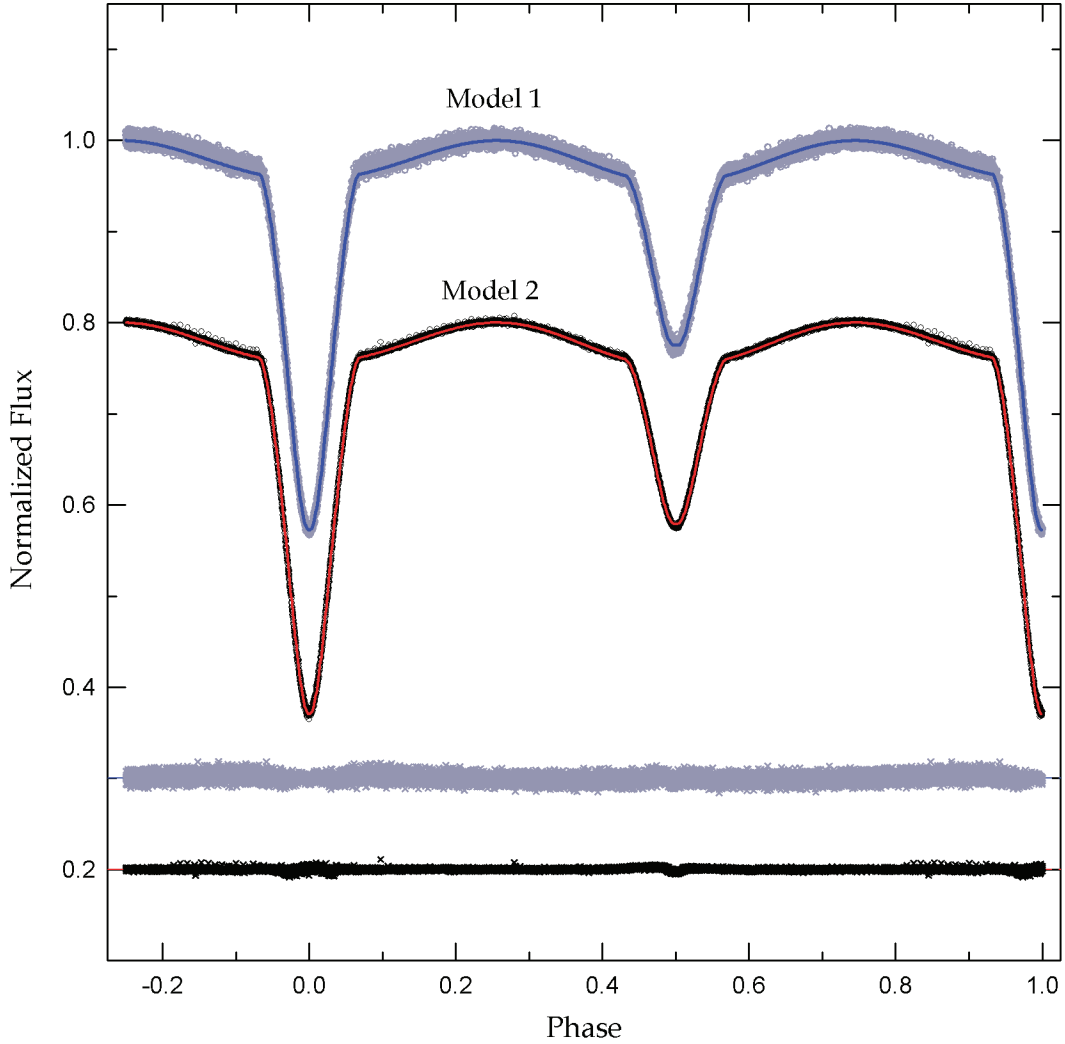


Fig. 2.— Binary light curve before (gray circle) and after (black circle) subtracting the pulsation signatures from the *Kepler* data. The blue and red solid curves are computed with the Model 1 and Model 2 parameters of Table 1, respectively. The corresponding residuals from the fits are offset from zero and plotted at the bottom in the same order as the light curves. In the light residuals from Model 2, some feature is certainly visible during the times of the secondary eclipse, which may come from insufficient removal of the pulsation effects in the orbital phases.

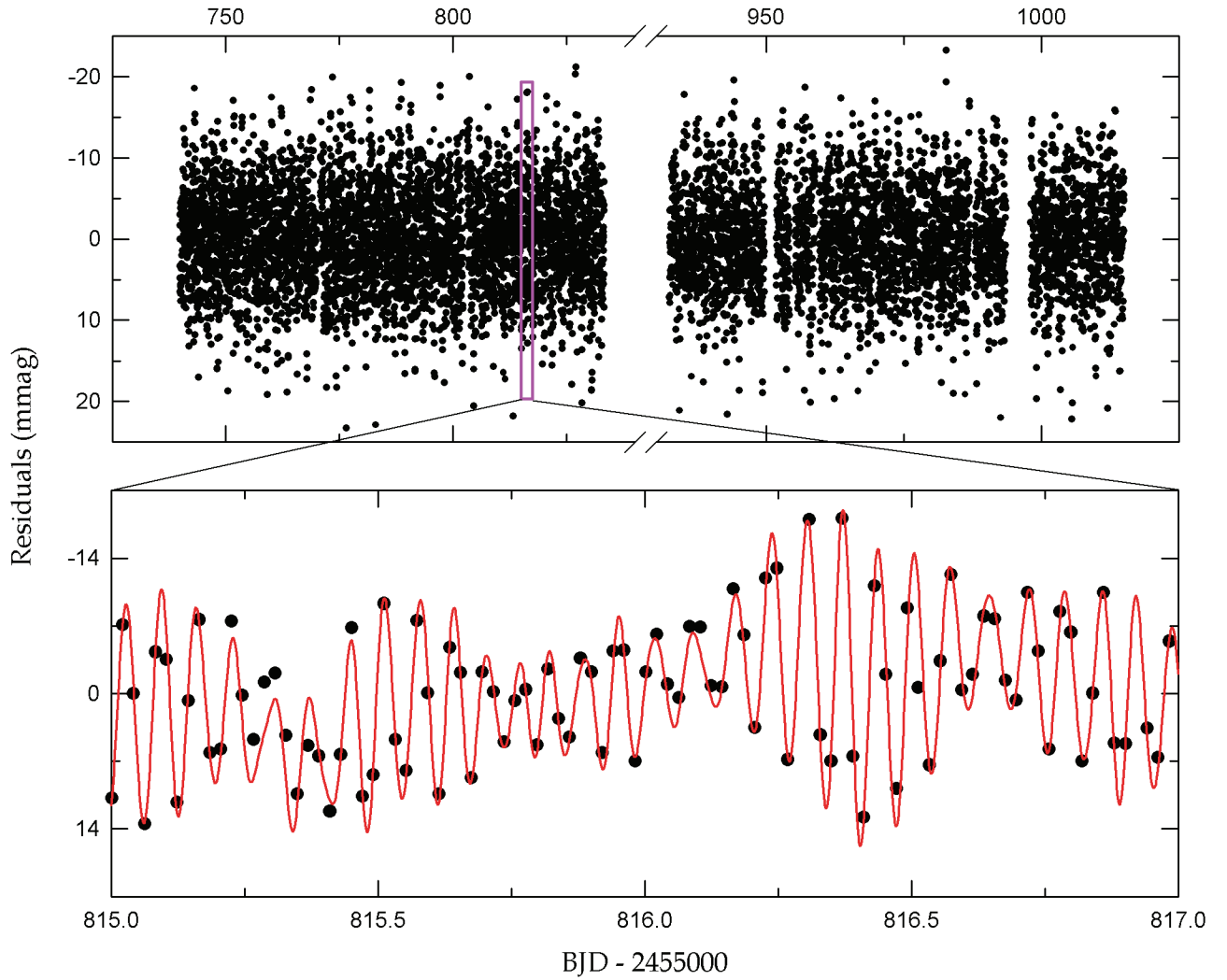


Fig. 3.— Light residuals after removing the binarity effects from the *Kepler* light curve. The lower panel presents a short section of the residuals marked by the inset box in the upper panel. The synthetic curve is computed from the 23-frequency fit to the data.

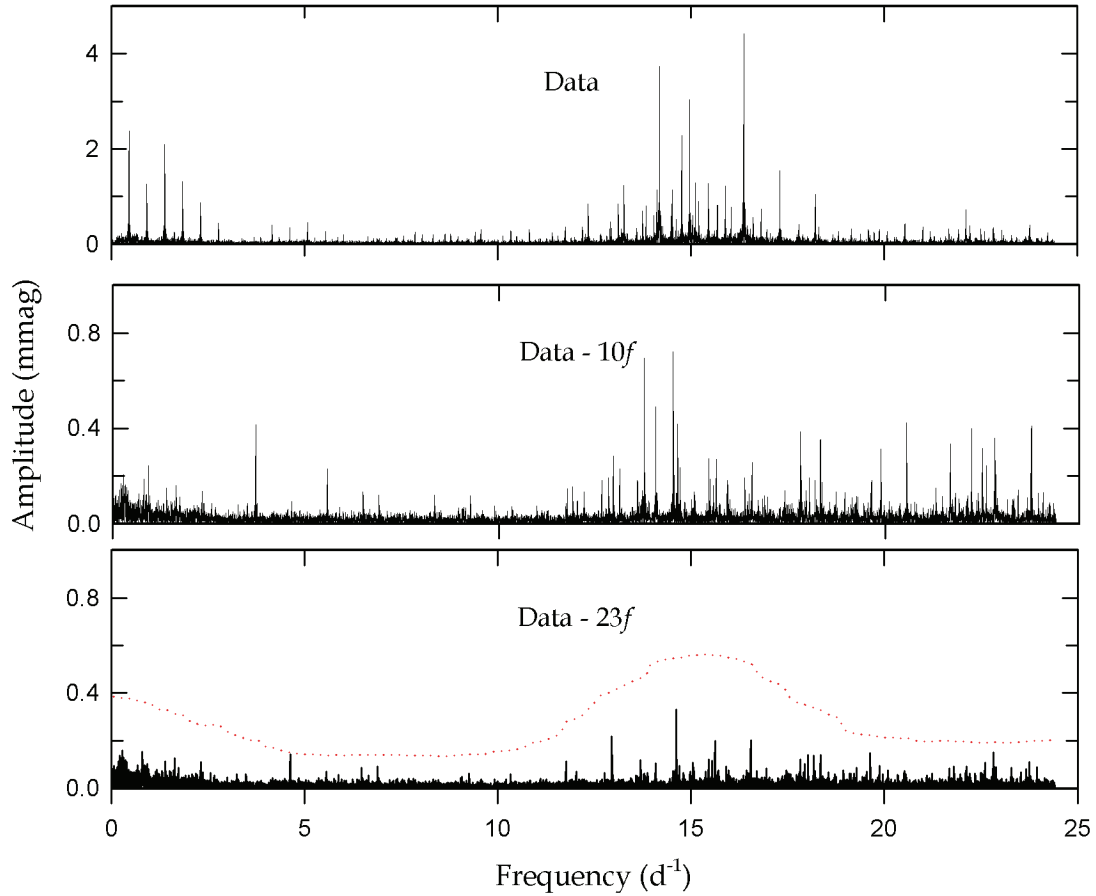


Fig. 4.— Amplitude spectra before (top panel) and after prewhitening the first 10 frequencies (middle panel) and all 23 frequencies (bottom panel) from the PERIOD04 program for the entire outside-eclipse residual data. The dotted line at the bottom panel corresponds to four times the noise spectrum, which was calculated for each frequency in an equidistant step of  $0.1 \text{ day}^{-1}$ .

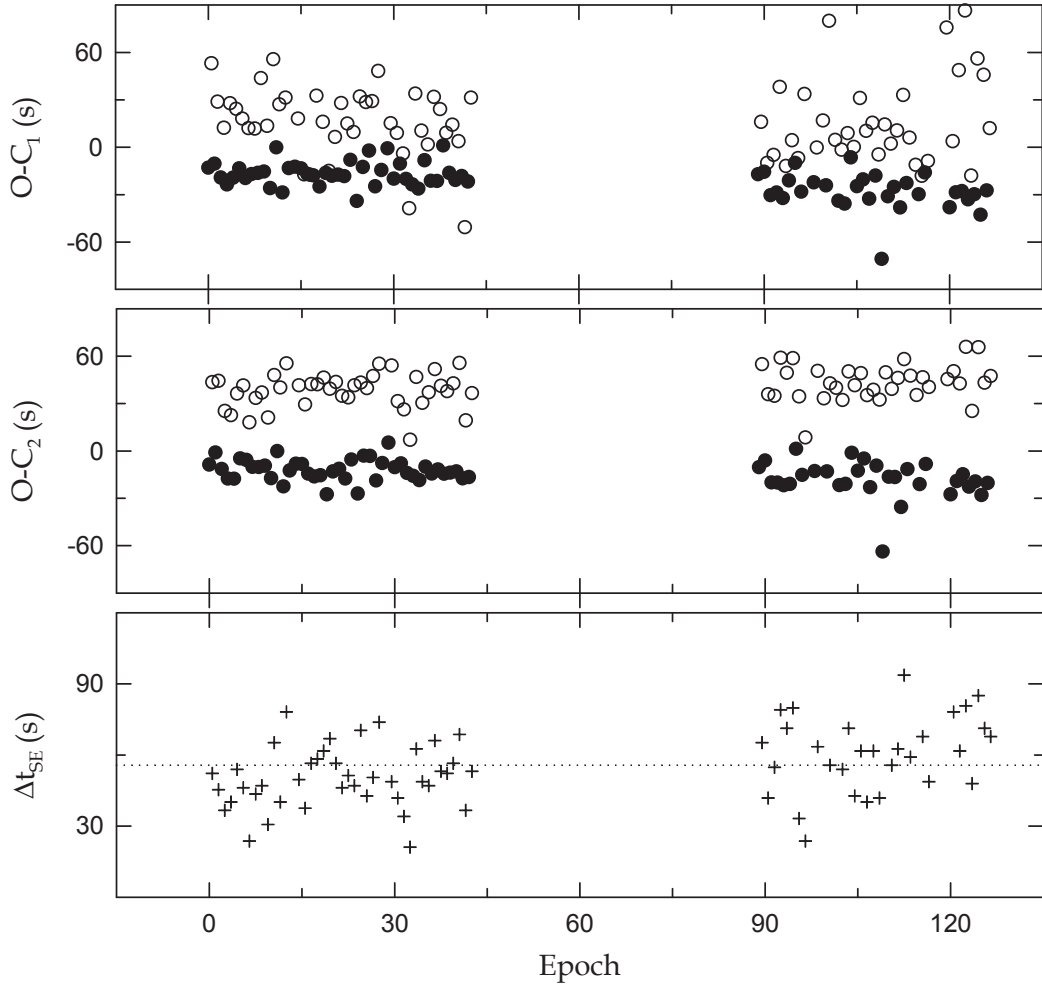


Fig. 5.—  $O-C$  diagrams of the minimum times measured from the observed (top panel) and pulsation-subtracted (middle panel) *Kepler* data. The filled and open circles represent the primary and secondary minima, respectively. Bottom panel shows the time delay ( $\Delta t_{SE}$ ) of the secondary eclipses related to one half period after the primary eclipses in the pulsation-subtracted data. The dotted line refers to the mean value of  $\Delta t_{SE} = 56 \pm 17$  s.

Table 1. Binary Parameters of KIC 11401845

Parameter	Model 1 <sup>a</sup>		Model 2 <sup>b</sup>	
	Primary	Secondary	Primary	Secondary
$T_0$ (BJD)	2,455,740.80720(13)		2,455,740.80729(5)	
$P$ (day)	2.1613895(18)		2.1613910(6)	
$q$	0.0699(16)		0.0695(10)	
$i$ (deg)	85.45(21)		85.10(12)	
$T$ (K)	7590	6217(26)	7590	6154(19)
$\Omega$	4.150(29)	1.879(7)	4.138(21)	1.873(4)
$\Omega_{\text{in}}$	1.861		1.860	
$A$	1.0	0.5	1.0	0.5
$g$	1.0	0.32	1.0	0.32
$X, Y$	0.671, 0.199	0.632, 0.232	0.671, 0.199	0.633, 0.229
$x, y$	0.599, 0.238	0.629, 0.280	0.599, 0.238	0.633, 0.278
$L/(L_1+L_2)$	0.7905(12)	0.2095	0.7940(8)	0.2060
$r$ (pole)	0.2450(13)	0.1638(29)	0.2457(10)	0.1651(19)
$r$ (point)	0.2474(14)	0.2083(78)	0.2481(10)	0.2136(56)
$r$ (side)	0.2470(14)	0.1695(32)	0.2476(10)	0.1710(21)
$r$ (back)	0.2473(14)	0.1928(49)	0.2480(10)	0.1956(32)
$r$ (volume) <sup>c</sup>	0.2464(14)	0.1753(43)	0.2471(10)	0.1771(29)
$\sum W(O - C)^2$	0.0050		0.0016	
Absolute parameters:				
$M$ ( $M_\odot$ )	1.70(8)	0.119(7)	1.70(8)	0.118(6)
$R$ ( $R_\odot$ )	2.11(5)	1.50(5)	2.12(4)	1.52(4)
$\log g$ (cgs)	4.02(3)	3.16(4)	4.02(3)	3.15(3)
$L$ ( $L_\odot$ )	13(2)	3.0(4)	13(2)	3.0(4)
$M_{\text{bol}}$ (mag)	1.92(12)	3.53(16)	1.92(12)	3.55(15)
BC (mag)	0.03(1)	-0.02(2)	0.03(1)	-0.03(2)
$M_V$ (mag)	1.89(12)	3.55(16)	1.89(12)	3.58(15)

<sup>a</sup>Result from the observed data.

<sup>b</sup>Result from the pulsation-subtracted data.

<sup>c</sup>Mean volume radius.



Table 2. Multiple Frequency Analysis of KIC 11401845

	Frequency (day <sup>-1</sup> )	Amplitude (mmag)	Phase (rad)	S/N	$Q$ (days)	Remark
$f_1$	16.37811±0.00004	4.41±0.23	5.74±0.15	33.13	0.026	
$f_2$	14.19519±0.00004	3.74±0.23	2.06±0.18	27.93	0.030	
$f_3$	14.97171±0.00005	3.18±0.24	5.18±0.22	22.85	0.028	
$f_4$	0.46268±0.00003	3.54±0.16	5.73±0.13	37.42		$f_{\text{orb}}$
$f_5$	14.76672±0.00007	2.28±0.24	2.63±0.30	16.56	0.029	
$f_6$	1.85072±0.00005	1.81±0.13	5.33±0.21	23.56		$4f_{\text{orb}}$
$f_7$	14.12286±0.00014	1.17±0.23	3.79±0.57	8.78	0.030	
$f_8$	15.20396±0.00019	0.90±0.24	4.42±0.78	6.45	0.028	
$f_9$	2.77609±0.00007	1.11±0.11	0.95±0.30	16.92		$6f_{\text{orb}}$
$f_{10}$	22.12255±0.00008	0.73±0.08	1.13±0.33	14.99	0.019	
$f_{11}$	14.50213±0.00023	0.74±0.23	3.76±0.93	5.41	0.029	$3f_3 - 2f_8$
$f_{12}$	13.75268±0.00021	0.69±0.20	3.11±0.85	5.90	0.031	
$f_{13}$	14.04653±0.00030	0.55±0.23	1.53±1.20	4.16	0.030	$f_3 - 2f_{\text{orb}}$
$f_{14}$	20.54260±0.00016	0.41±0.09	5.00±0.64	7.87	0.021	$f_1 + 9f_{\text{orb}}$
$f_{15}$	3.70145±0.00012	0.52±0.09	2.88±0.48	10.35		$8f_{\text{orb}}$
$f_{16}$	22.22705±0.00015	0.40±0.08	3.22±0.61	8.18	0.019	$2f_7 - 13f_{\text{orb}}$
$f_{17}$	23.77410±0.00015	0.40±0.08	0.08±0.62	8.11	0.018	
$f_{18}$	17.79523±0.00029	0.38±0.15	4.34±1.19	4.21	0.024	
$f_{19}$	22.82621±0.00017	0.36±0.08	3.22±0.68	7.34	0.019	
$f_{20}$	21.67877±0.00018	0.35±0.08	2.34±0.71	7.03	0.020	
$f_{21}$	18.31316±0.00030	0.33±0.14	4.19±1.23	4.07	0.023	
$f_{22}$	22.50255±0.00019	0.31±0.08	6.20±0.77	6.49	0.019	
$f_{23}$	19.87857±0.00021	0.31±0.09	3.96±0.87	5.79	0.021	

Table 3. Eclipse Timings Measured from Both Datasets Including and Removing the pulsations

Observed Data			Epoch	Min	Pulsation-Subtracted Data		
BJD	Error	$O-C_1$			BJD	Error	$O-C_2$
2,455,740.80714	$\pm 0.00031$	$-0.000150$	0.0	I	2,455,740.80719	$\pm 0.00014$	$-0.000100$
2,455,741.88860	$\pm 0.00120$	$+0.000615$	0.5	II	2,455,741.88849	$\pm 0.00028$	$+0.000504$
2,455,742.96856	$\pm 0.00064$	$-0.000121$	1.0	I	2,455,742.96867	$\pm 0.00039$	$-0.000011$
2,455,744.04971	$\pm 0.00083$	$+0.000334$	1.5	II	2,455,744.04989	$\pm 0.00031$	$+0.000514$
2,455,745.12985	$\pm 0.00038$	$-0.000222$	2.0	I	2,455,745.12994	$\pm 0.00025$	$-0.000132$
2,455,746.21091	$\pm 0.00064$	$+0.000142$	2.5	II	2,455,746.21106	$\pm 0.00020$	$+0.000293$
2,455,747.29119	$\pm 0.00050$	$-0.000273$	3.0	I	2,455,747.29126	$\pm 0.00020$	$-0.000203$
2,455,748.37248	$\pm 0.00162$	$+0.000322$	3.5	II	2,455,748.37242	$\pm 0.00034$	$+0.000262$
2,455,749.45263	$\pm 0.00030$	$-0.000224$	4.0	I	2,455,749.45265	$\pm 0.00028$	$-0.000204$
2,455,750.53383	$\pm 0.00052$	$+0.000281$	4.5	II	2,455,750.53397	$\pm 0.00019$	$+0.000421$

Note. — This table is available in its entirety in machine-readable and Virtual Observatory (VO) forms in the online journal. A portion is shown here for guidance regarding its form and content.